ALEPH 95-048
PHYSIC 95-044
A. Trabelsi et al.
26 April 1995

ALEPH

W mass reconstruction in the $WW \to \ell\bar{\nu}q_1\bar{q}_2$ channel

A. Trabelsi[1] , P. Perez[2] , J. Schwindling [3]

DAPNIA/SPP
CE Saclay
91191 GIF sur YVETTE CEDEX
FRANCE

[1]TRABELSI @ frcpn11.in2p3.fr
[2]PEREZ @ frcpn11.in2p3.fr
[3]JEROME @ frcpn11.in2p3.fr

Contents

1 Introduction

The measurement of the W mass by direct invariant mass reconstruction in the $WW \to \ell\bar{\nu}q_1\bar{q}_2$ channel will be of particular interest at LEP2 because:

- The clean topology of the events, with a high energy lepton and a large missing momentum recoiling against a hadronic system, will lead to a high selection efficiency with a low background level.
- The particles will not be mixed up between the two W's (as in 4 jet events).
- There will be no combinatorial background, as it is the case in the 4 jet channel where one of the three jet-jet combinations has to be chosen.
- There will be no colour reconnection effects between the two W's.
- There will be no Bose-Einstein effect between the two W's.
- The sign of the W's will be known, allowing to compare m_{W^+} and m_{W^-}.

This note presents an analysis of the W mass reconstruction in the $WW \to \ell\bar{\nu}q_1\bar{q}_2$ channel. Section 2 presents the Monte-Carlo samples used in this study. Section 3 presents the selection procedure both in the $WW \to e,\mu\bar{\nu}q_1\bar{q}_2$ and the $WW \to \tau\bar{\nu}q_1\bar{q}_2$ channels. Section 4 deals with the event fit using the constrained fit method, then, in Section 5, we will deal with the fit of the mass distribution and the results, and finally the conclusion.

2 Monte Carlo samples

Samples of $e^+e^- \to W^+W^-$ at different W masses and center of mass energies (see table 1) were generated using PYTHIA 5.6 and JETSET 7.3, and processed through GALEPH and JULIA(1993 geometry, no SICAL). Various background processes were also generated at $\sqrt{s} = 176$ GeV, using the same generator. These samples are described in table 2. The gamma-gamma events, $e^+e^- \to \gamma^*\gamma^*e^+e^-$, are generated requiring a hadronic mass of more than 20 GeV/c^2.

m_W	165 GeV			176 GeV			190 GeV		
(GeV/c^2)	Events	L	σ (pb)	Events	L	σ (pb)	Events	L	σ (pb)
80.00				25000	1620	**15.4**			
80.25	25000	2810	**8.89**	50000	3200	**15.2**	25000	1410	**17.7**
80.50				25000	1690	**14.8**			

Table 1: Number of $e^+e^- \to W^+W^-$ events, integrated luminosity, L, (in pb^{-1}) and cross-section, generated using PYTHIA 5.6 and JETSET 7.3.

Background	Events	Luminosity (pb^{-1})	Cross section (pb)
$e^+e^- \to q\bar{q}(\gamma)$	40000	325	123
$e^+e^- \to Ze^+e^-$	2500	862	2.9
$e^+e^- \to ZZ$	2000	4440	0.46
$e^+e^- \to We\bar{\nu}$	2500	3570	0.70
$e^+e^- \to \gamma^*\gamma^*e^+e^-$	100000	187	535

Table 2: Background events generated using PYTHIA 5.6 and JETSET 7.3 at 176 GeV.

3 Event Selection

As the τ lepton decays into a neutrino and one or more charged particles (plus possibly neutral hadrons), its identification is more difficult than the identification of e and μ leptons. So, in this study, the $WW \to e, \mu\bar{\nu}q_1\bar{q}_2$ events and the $WW \to \tau\bar{\nu}q_1\bar{q}_2$ events are selected separately.

3.1 $WW \to e, \mu\bar{\nu}q_1\bar{q}_2$ events

To select these events channel the following set of cuts is used:

- The number, N_{ch}, of "good" charged tracks (defined by a requirement of at least 4 TPC coordinates and a distance to the interaction point of less than 2.5 cm in the transverse direction and 7 cm in the longitudinal direction) is required to be $5 \leq N_{ch} \leq 33$. This cut removes most of $WW \to \ell\bar{\nu}\ell'\bar{\nu}'$ events as well as two (and four) lepton events, and part of the $WW \to q_1\bar{q}_2q_3\bar{q}_4$ events, as shown in figure 1.
- The total transverse momentum, P_t, with respect to the beam axis must be greater than 5% of the center of mass energy, $\sqrt{s}$, (figure 2). This removes most of the remaining $WW \to q_1\bar{q}_2q_3\bar{q}_4$ and $e^+e^- \to q\bar{q}(\gamma)$ background.
- The total longitudinal momentum, P_l, with respect to the beam axis must be less than 30% of $\sqrt{s}$,(figure 3). This removes part of the $e^+e^- \to q\bar{q}(\gamma)$ and $e^+e^- \to Ze^+e^-$ backgrounds. Without this cut, the $e^+e^- \to q\bar{q}(\gamma)$ background, after all other cuts, would be 20 % higher.

For each event the most energetic good charged track (with more than 5 GeV) is selected. If it is identified as an electron with more than 1 GeV, all photons within 1° are added to the track in order to include bremsstrahlung effects. Then the following cuts are applied:

- Figure 4 shows the distribution of the energy of the selected track, E_{max}, for the $WW \to e, \mu\bar{\nu}q_1\bar{q}_2$, $WW \to \tau\bar{\nu}q_1\bar{q}_2$ events and the $e^+e^- \to q\bar{q}(\gamma)$, $e^+e^- \to We\bar{\nu}$ backgrounds. The low energy tail in the $WW \to e, \mu\bar{\nu}q_1\bar{q}_2$ channel is due to events where the selected track does not correspond to the real lepton.

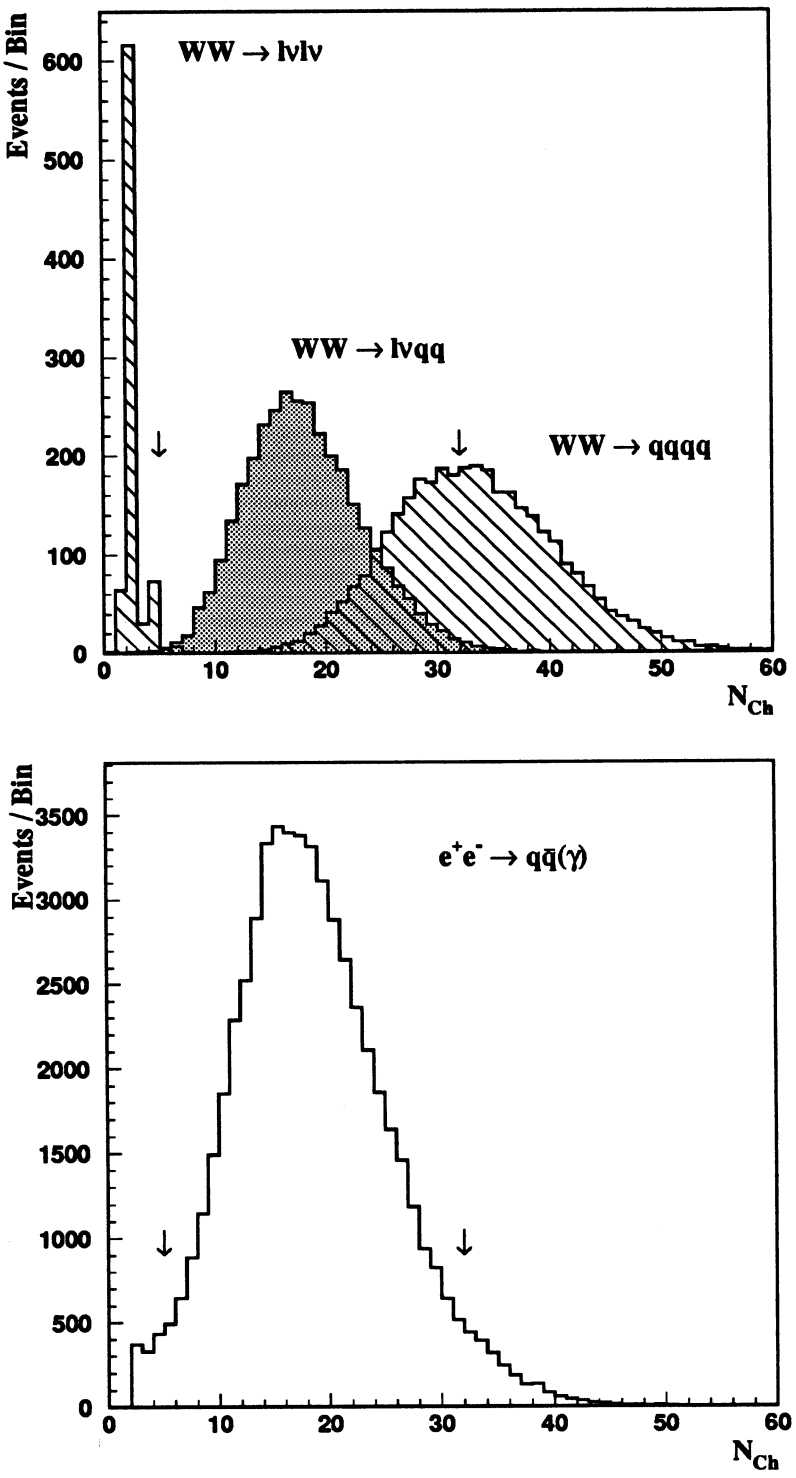

Figure 1: Number of charged tracks for the $e^+e^- \to W^+W^-$ events and $e^+e^- \to q\bar{q}(\gamma)$ background, for 500 pb^{-1}.

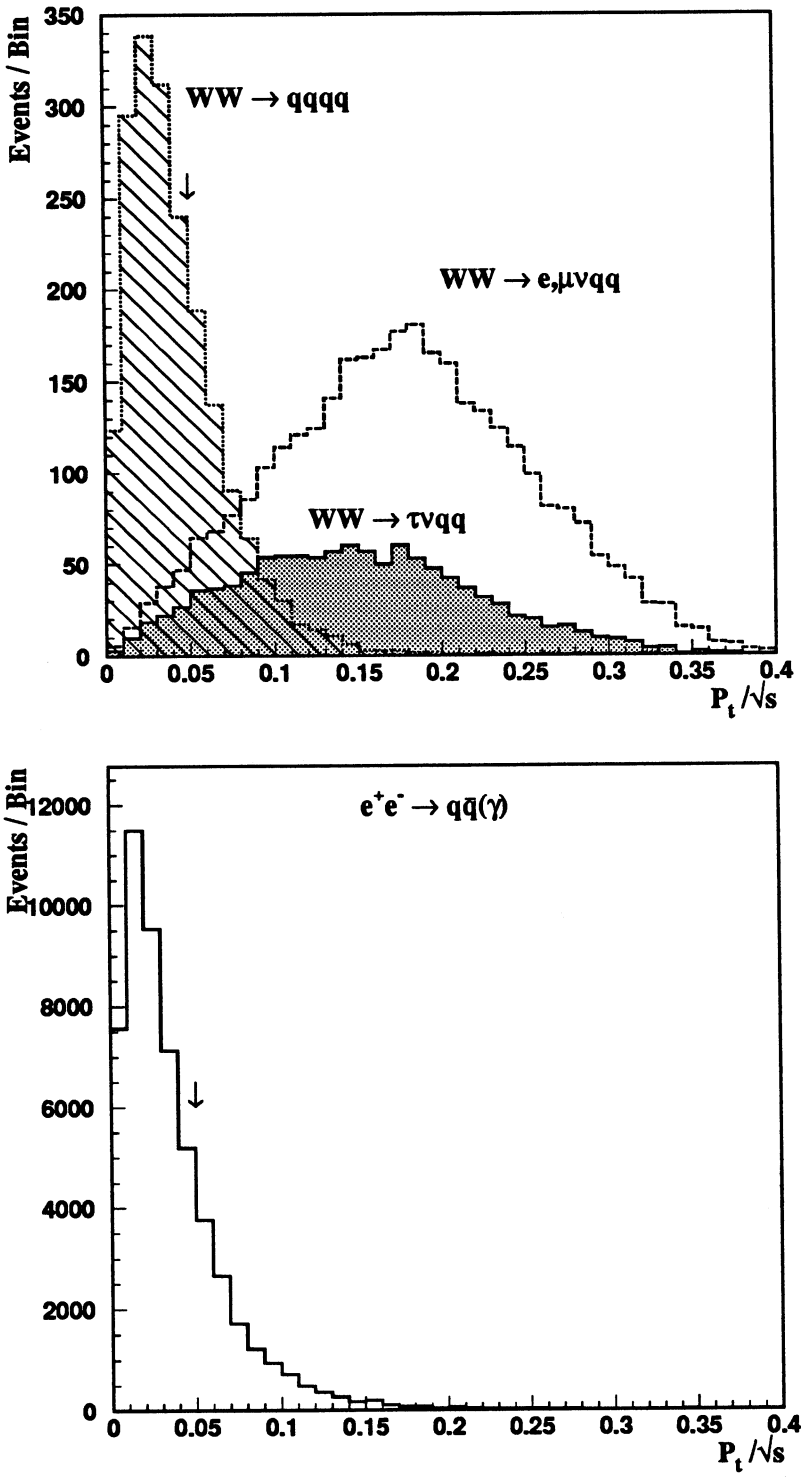

Figure 2: Ratio of the transverse momentum to the LEP energy for the signal events and the $e^+e^- \to q\bar{q}(\gamma)$ background, after the cut on the number of charged tracks, for 500 pb^{-1}.

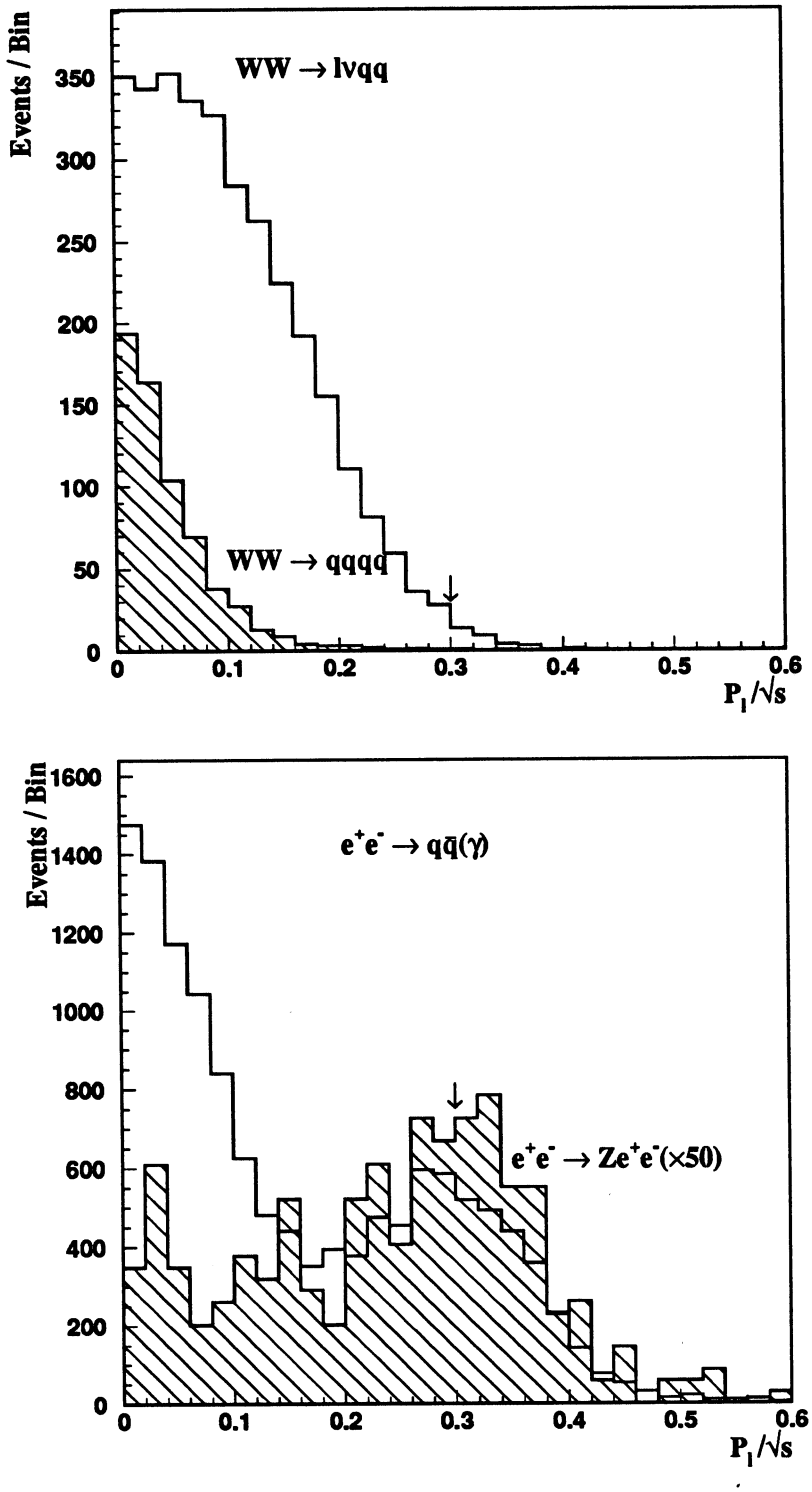

Figure 3: Distribution of the ratio of the longitudinal momentum to the LEP energy, for the signal events, and, the backgrounds $e^+e^- \to q\bar{q}(\gamma)$ and $e^+e^- \to Ze^+e^-$, after the two previous cuts, for 500 pb^{-1}.

E_{max} is required to be more than 22 GeV, this removes most of remaining $WW \to \tau\bar{\nu}q_1\bar{q}_2$, $e^+e^- \to We\bar{\nu}$ and $e^+e^- \to q\bar{q}(\gamma)$ background events. The peak at 88 GeV is due to tracks with bad χ^2 and very high reconstructed energy that had been set to $\sqrt{s}/2$ by ENFLW.

- The selected track must be identified, by ENFLW, as a lepton (electron or muon). As in most $e^+e^- \to q\bar{q}(\gamma)$ and $WW \to q_1\bar{q}_2q_3\bar{q}_4$ events the selected track is expected to be a hadron, a large part of these backgrounds is removed. This requirement insures that the remaining $WW \to \tau\bar{\nu}q_1\bar{q}_2$ events are those where the τ decays into an e or a μ so that all the decay products of the τ are identified and separated from the other W decay products.

- The lepton is removed from the event and all other particles are assigned to the "hadronic" W. Figure 5 shows the ratio of the W energy, E_W, to the beam energy. This ratio is requested to be equal to 1 within 30% (which corresponds to $\pm 3\sigma$). This cut removes part of the remaining $e^+e^- \to ZZ$ background (where there is no missing energy due to the ν as in signal events).

- The lepton isolation is the angle, θ_{iso}, between the lepton and the nearest good charged track. Only events with $\theta_{iso} > 7^o$ are kept (figure 6).

The efficiency and the background discrimination (only $e^+e^- \to q\bar{q}(\gamma)$ is shown here) after each cut are shown in table 3. The errors are only statistical.

Cuts	$e^+e^- \to W^+W^-$				$e^+e^- \to q\bar{q}(\gamma)$
	$e,\mu\nu qq$	$\tau\nu qq$	$l\nu l\nu$	$qqqq$	
	14604	7288	5248	22813	40000
$5 \le N_{ch} \le 33$	14533	7248	85	12721	35104
$P_t/\sqrt{s} \ge .05$	14169	6723	79	4105	8528
$P_l/\sqrt{s} \le .3$	13985	6686	72	4099	6941
e or μ	12376	1363	39	232	902
$E_{max} \ge 22$ GeV	12244	579	34	47	314
$.7 \le E_W/E_b \le 1.3$	12036	568	1	2	108
$\theta_{iso} \ge 7^o$	11537	511	0	0	24
For 500 pb^{-1}	**1753 ± 16**	**78 ± 3.4**	**<.5**	**<.5**	**37 ± 7.5**

Table 3: Number of signal events and $e^+e^- \to q\bar{q}(\gamma)$ background after each cut at $\sqrt{s} = 176$ GeV

Most of the significant background processes are studied. Table 4 shows the numbers of expected events from each background source for 500 pb^{-1} at $\sqrt{s}$=176 GeV. The total number of expected background events is 71 which corresponds to 3.7% of the selected events. The $WW \to \tau\bar{\nu}q_1\bar{q}_2$ events are not considered as background for the $WW \to e,\mu\bar{\nu}q_1\bar{q}_2$ channel, because only events where the τ decays in to a μ or an e are kept. So they are similar, in some way, to $WW \to e,\mu\bar{\nu}q_1\bar{q}_2$ where the lepton momentum is badly measured. One can also note that $e^+e^- \to Ze^+e^-$ and $e^+e^- \to We\bar{\nu}$ backgrounds affect only the $WW \to e\bar{\nu}q_1\bar{q}_2$ channel.

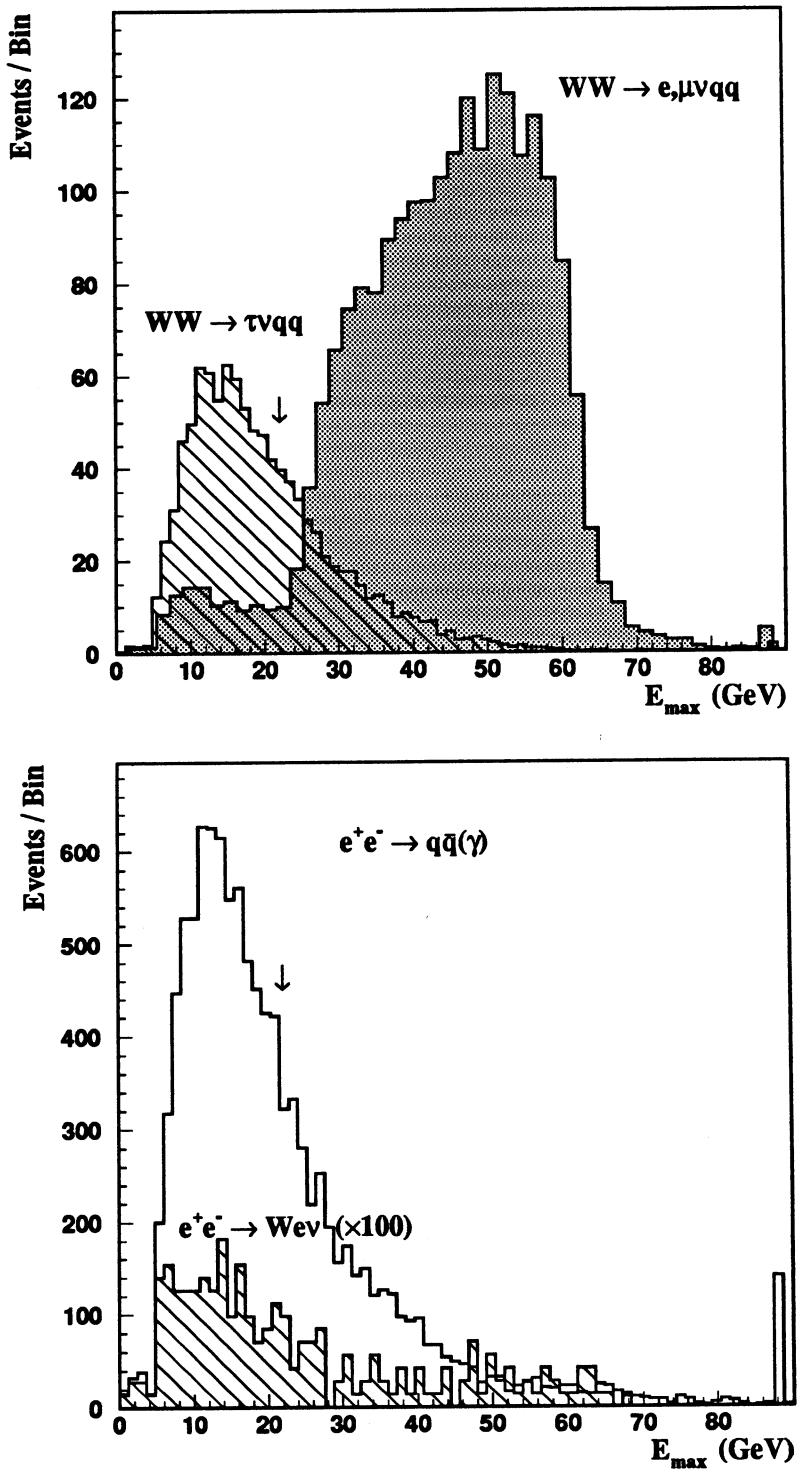

Figure 4: Energy distribution of the most energitic charged track in the event for $WW \to e, \mu\bar{\nu}q_1\bar{q}_2$ and $WW \to \tau\bar{\nu}q_1\bar{q}_2$ events, and, $e^+e^- \to q\bar{q}(\gamma)$ and $e^+e^- \to We\bar{\nu}$ backgrounds, after previous cuts, for 500 pb^{-1}.

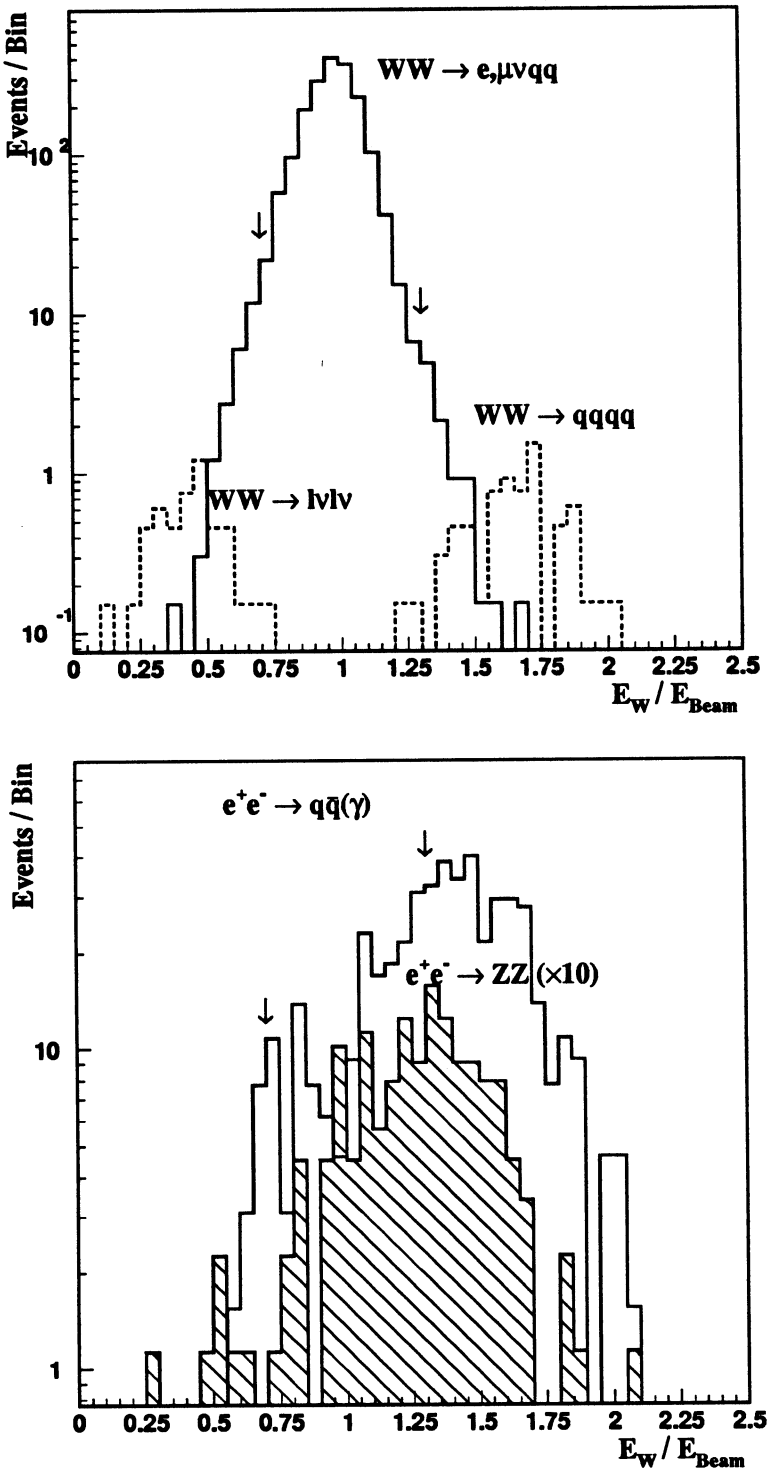

Figure 5: Ratio of the W energy to the beam energy the signal events, and, the $e^+e^- \to q\bar{q}(\gamma)$ and $e^+e^- \to ZZ$ backgrounds, for 500 pb^{-1}.

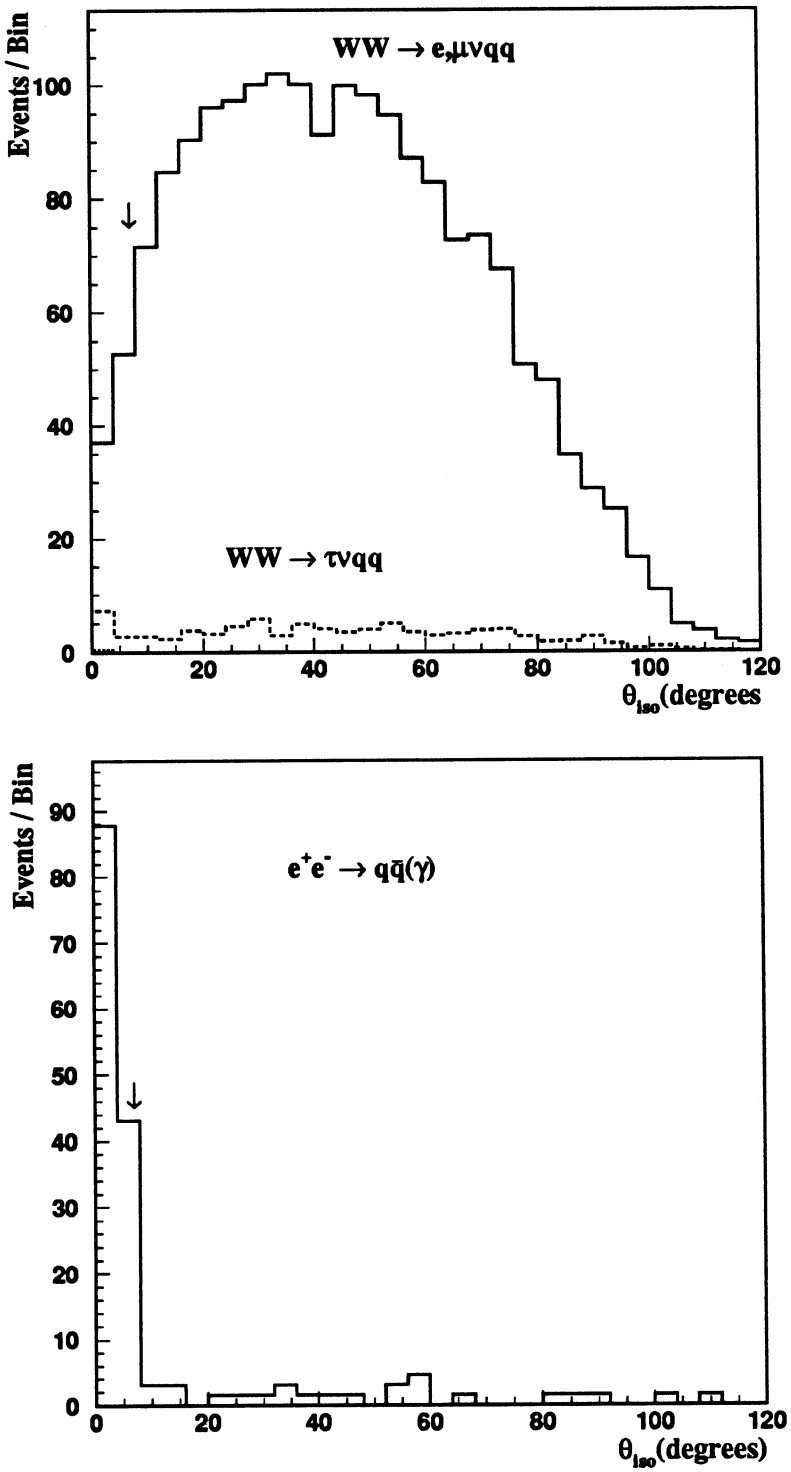

Figure 6: Distribution of the isolation angle of the selected lepton for the signal and $e^+e^- \to q\bar{q}(\gamma)$ background, after previous cuts, for 500 pb^{-1}.

Background	All the sample	**For 500 pb^{-1}**
$e^+e^- \to q\bar{q}(\gamma)$	24	**37 ± 7.5**
$e^+e^- \to Ze^+e^-$	37	**21 ± 3.5**
$e^+e^- \to ZZ$	62	**7 ± 0.9**
$e^+e^- \to We\bar{\nu}$	40	**6 ± 0.9**
$e^+e^- \to \gamma^*\gamma^*e^+e^-$	0	**<8 at 95% CL**
$WW \to \ell\bar{\nu}\ell'\bar{\nu}'$	0	**<.5 at 95% CL**
$WW \to q_1\bar{q}_2q_3\bar{q}_4$	0	**<.5 at 95% CL**
		71 ± 8.4

Table 4: Number of background events expected for 500 pb^{-1} at $\sqrt{s}$=176 GeV

Supposing that the selection efficiency for background is independent of the center of mass energy, we estimate the number of these events for other values of $\sqrt{s}$. Table 5 shows the estimated numbers of background events for 500 pb^{-1}. The total number of these events is almost constant, but as the cross-section of the $e^+e^- \to W^+W^-$ process increases with $\sqrt{s}$, the purity is better for higher energies. For comparison, a sample of $e^+e^- \to ZZ$ events at 190 GeV was generated: the number of selected events is of the same order as the estimated one.

LEP energy	165 GeV	176 GeV	190 GeV
$e^+e^- \to q\bar{q}(\gamma)$	45	**37 ± 7.5**	31
$e^+e^- \to Ze^+e^-$	19	**21 ± 3.5**	23
$e^+e^- \to ZZ$	7	**7 ± 0.9**	17 (**10.8 ± 1.4**)
$e^+e^- \to We\bar{\nu}$	5	**6 ± 0.9**	7
All background	86	**71 ± 8.4**	78
contamination	7.3 %	**3.7 ± .4 %**	3.5 %

Table 5: Estimated numbers of background events as a function of the center of mass energy (**using generated events**), for 500 pb^{-1}.

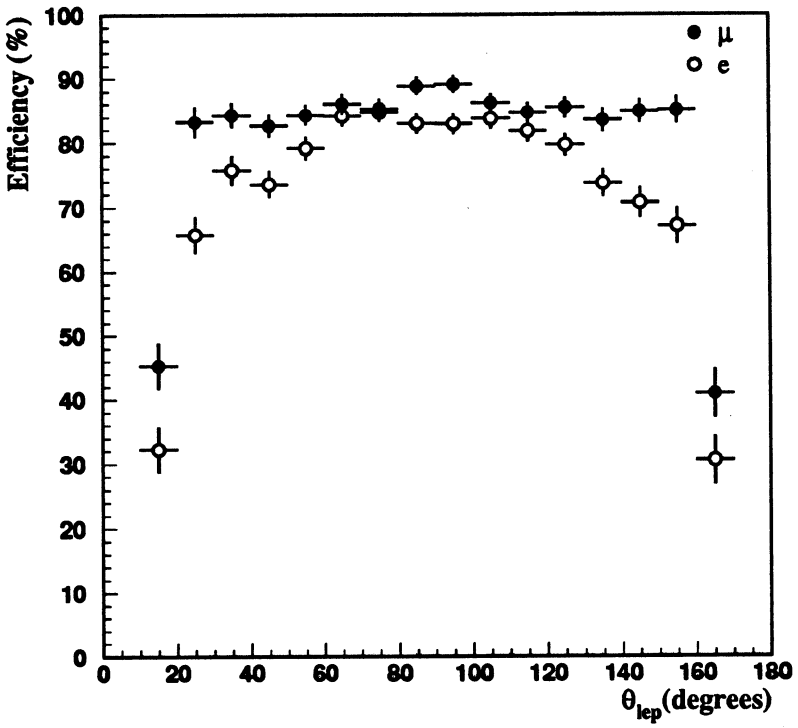

Figure 7: Efficiency of the selection as a function of lepton's polar angle for the $WW \to e, \mu\bar{\nu}q_1\bar{q}_2$ channel.

3.2 $WW \to \tau\bar{\nu}q_1\bar{q}_2$ events

Events selected in the previous section are removed from the sample. As the τ lepton decays in 63% of the cases into ν+*hadrons*, the previous cuts are not suited for an optimized selection for this channel. The same variables, as above, are used, but, in most cases, with tighter cuts:

- $5 \leq N_{ch} \leq 33.$
- $P_t/\sqrt{s} \geq .075$
- $P_l/\sqrt{s} \leq .4$

The most isolated good charged track with more than 5 GeV is selected. If it is identified as an electron all photons within 2^o are added vectorially to the track in order to include bremsstrahlung effects. If it is not identified as a lepton, all neutral hadrons within 5^o are added to the track. The energy of the reconstructed particle is required to be at least 10 GeV.

- $.8 \leq E_W/E_b \leq 1.2$
- $\theta_{iso} > 22^o$

The efficiency of each cut is shown in table 6. The last cut removes more than half of the signal events, but such a severe cut reduces the $e^+e^- \to q\bar{q}(\gamma)$ background by a factor 50. As the most isolated track is selected, a so severe cut is necessry to reduce the background level. Also, the fact that only 1-prong τ are selected here reduces the signal selection efficiency. Part of $WW \to e, \mu\bar{\nu}q_1\bar{q}_2$ events are selected with this set of cuts. These events are those whom e or μ is missidentified or those with $.3 < P_l/\sqrt{s} \leq .4$.

As shown in Table 7 the total number of background events for 500 pb^{-1} at $\sqrt{s} = 176$ GeV is 38 which corresponds to a purity of 91.7 %. Table 8 shows the estimated numbers for background events for two other center of mass energies. The contamination of the selected events is lower for higher energies.

Cuts	$e^+e^- \to W^+W^-$				$e^+e^- \to q\bar{q}(\gamma)$
	$\tau\nu qq$	$e, \mu\nu qq$	$l\nu l\nu$	$qqqq$	
	6777	3067	5248	22813	39976
$5 \leq N_{ch} \leq 33$	6737	2996	85	12721	35080
$P_t/\sqrt{s} \geq .075$	5691	2499	70	1638	3744
$P_l/\sqrt{s} \leq .4$	5689	2486	70	1636	3606
$E_{max} \geq 10$ GeV	5426	2415	68	1621	3436
$.8 \leq E_W/E_b \leq 1.2$	4059	1668	4	12	895
$\theta_{iso} \geq 22^o$	1886	869	1	4	17
For 500 pb^{-1}	**287 ± 2.5**	**132 ± 1.7**	**<1**	**<1.5**	**26 ± 6.3**

Table 6: Number of signal events and $e^+e^- \to q\bar{q}(\gamma)$ background after each cut at $\sqrt{s}$ =176 GeV. Initial samples do not include events selected previously.

Background	All the sample	**For 500 pb^{-1}**
$e^+e^- \to q\bar{q}(\gamma)$	17	**26 ± 6.3**
$e^+e^- \to Ze^+e^-$	8	**4.6 ± 1.6**
$e^+e^- \to ZZ$	22	**2.5 ± 0.5**
$e^+e^- \to We\bar{\nu}$	34	**5 ± 0.8**
$e^+e^- \to \gamma^*\gamma^*e^+e^-$	0	**<8 at 95% CL**
$WW \to \ell\bar{\nu}\ell'\bar{\nu}'$	1	**<1. at 95% CL**
$WW \to q_1\bar{q}_2q_3\bar{q}_4$	4	**<1.5 at 95% CL**
		38 ± 6.6

Table 7: Number of background events expected for 500 pb^{-1} at $\sqrt{s}$=176 GeV

Tables 9 and 10 show the efficiency of selection for the $WW \to e, \mu\bar{\nu}q_1\bar{q}_2$ and $WW \to \tau\bar{\nu}q_1\bar{q}_2$ channels (adding events selected by the two sets of cuts). As shown in these tables the efficiency for the $WW \to e, \mu\bar{\nu}q_1\bar{q}_2$ channel is about 85% independent of the center of mass energy and the W mass, while the efficiency for the $WW \to \tau\bar{\nu}q_1\bar{q}_2$ channel is much lower, 33%, and increases as $\sqrt{s}$ increases (this is due to the higher energy of τ decay products). Figure 7 shows the $WW \to e, \mu\bar{\nu}q_1\bar{q}_2$ selection efficiency as a function of the lepton poalr angle. The overall selection efficiency is larger for muons than for electrons (Figure 7 reveals that the selection efficiency is related to the lepton identification which is slightly better for the muons).

LEP energy	165 GeV	176 GeV	190 GeV
$e^+e^- \to q\bar{q}(\gamma)$	32	**26 ± 6.3**	22
$e^+e^- \to Ze^+e^-$	4	**4.6 ± 1.6**	5
$e^+e^- \to ZZ$	2.5	**2.5 ± 0.5**	6 (**5.7 ± 1.**)
$e^+e^- \to We\bar{\nu}$	4	**5 ± 0.8**	6
All background	43	**38 ± 6.6**	39
contamination	16.5 %	**8.3 ± 1.4 %**	6.9 %

Table 8: Estimated numbers of background events as a function of the center of mass energy (**using generated events**), for 500 pb^{-1}.

LEP energy	165 GeV	176 GeV	190 GeV
$WW \to e,\mu\bar{\nu}q_1\bar{q}_2$	1121 ± 14	1885 ± 17	2168 ± 28
	85.0 ± 0.4 %	**84.9 ± 0.3 %**	**84.3 ± 0.4 %**
$WW \to \tau\bar{\nu}q_1\bar{q}_2$	193 ± 5.9	365 ± 7.4	480 ± 13
	30.0 ± .8 %	**32.9 ± .5 %**	**36.5 ± .8 %**

Table 9: Numbers of selected signal events and efficiencies for $WW \to e,\mu\bar{\nu}q_1\bar{q}_2$ and $WW \to \tau\bar{\nu}q_1\bar{q}_2$ as a function of the center of mass energy, for 500 pb^{-1}.

W mass	80.00 GeV/c^2	80.25 GeV/c^2	80.50 GeV/c^2
$WW \to e,\mu\bar{\nu}q_1\bar{q}_2$	85.5 ± 0.4 %	84.9 ± 0.3 %	85.8 ± 0.4 %
$WW \to \tau\bar{\nu}q_1\bar{q}_2$	33.6 ± .8 %	32.9 ± .5 %	32.8 ± .8 %

Table 10: Efficiencies of selection for $WW \to e,\mu\bar{\nu}q_1\bar{q}_2$ and $WW \to \tau\bar{\nu}q_1\bar{q}_2$ events as a function of W mass at $\sqrt{s} = 176$ GeV.

4 Event Fit

Because of the finite energy resolution of the detector and the loss of particles (neutrinos, losses in the beam pipe and cracks,...) the event does not fulfil the kinematical constraints and some corrections to the momenta are needed.

The event, excluding the reconstructed lepton, is forced into two jets using a clustering algorithm (DURHAM). The missing 3-momentum is assigned to the neutrino[1]. Then the four 4-momenta (the two jets, the lepton and the neutrino) are fitted using the constrained fit method [2]. The KINGAL momenta are used to determine the covariance matrix for different parameters of the fit.

Figures 8 and 9 show the resolution on the parameter $a \simeq E^{\text{real}}/E^{\text{measured}}$ as a function of the measured energy and direction of the reconstructed particle. The jet resolution is about 10%, slightly improving with the measured energy. The resolution on the lepton energy is what is expected from $\sigma(1/P) \simeq .8 \times 10^{-3}(\text{GeV/c})^{-1}$. For small polar angles, jets loose part of their particles in the beam pipe, and the number of TPC coordinates per track is much smaller. Thus, resolutions worsen and energies are underestimated ($a > 1$). Figure 10 shows that for high energy, the energy is slightly overestimated ($a < 1$). The particular shapes of $\sigma(a)$ and $\langle a \rangle$ are due to the fact that they are functions of the measured energy (used in the fit), instead of the real energy. This shape is a convolution of the detector resolutions by the energy spectrum (same as figure 4).

Using Monte-Carlo events, a parameterized covariance matrix, $\mathbf{V}(E_i, \theta_i)$, is obtained.

In the 4-constrained fit only the energy and the momentum conservation is requested. ISR photons are not taken into account as the method cannot fit energies below few GeV. Figure 9 shows that after fit, the resolution on the jet and neutrino momenta is slightly improved. The mean value of the parameter a is closer to 1, which indicates a better energy reconstruction(figure 10). The fact that we use the momentum conservation to define the neutrino, reduces the performance of the method, as compared to the 4-jet channel [2].

The results are improved with the 5-constrained fit where the two W masses are requested to be equal.

$$\begin{cases} M_{W_1} = M_{W_2} \\ \vec{P}_{W_1} = \vec{P}_{W_2} \end{cases} \Leftrightarrow E_{W_1} = E_{W_2} = E_{beam} \tag{1}$$

To take into account the finite W width, $\Gamma_W = 2.11 \pm 0.03$ GeV/c^2, the fifth constraint is notwritten with a linear form [3] [4]:

$$f_5 = E_W - E_{beam} = 0 \tag{2}$$

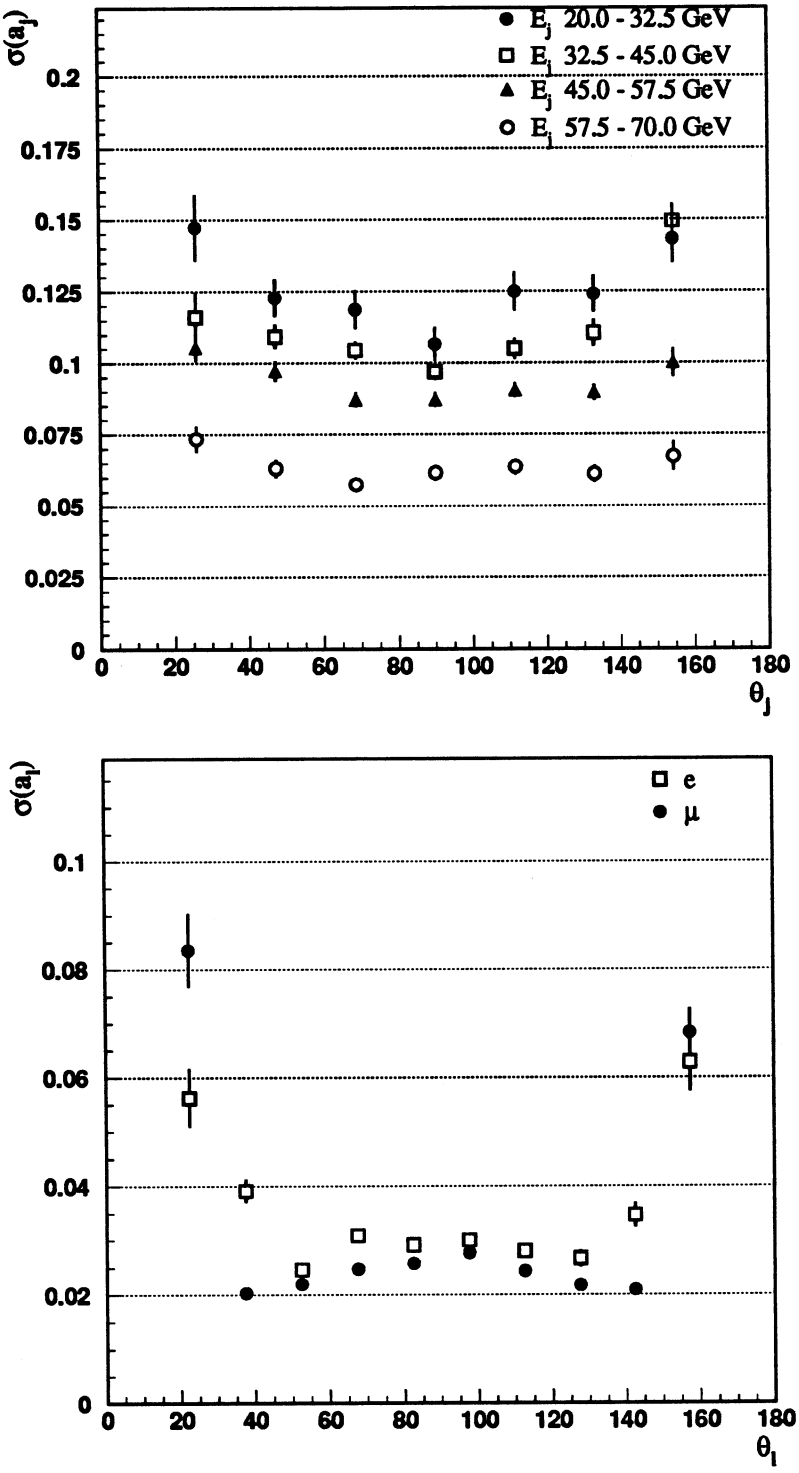

Figure 8: Resolution on the parameter **a** for jets and leptons in the $WW \to e, \mu\bar{\nu}q_1\bar{q}_2$ channel as a function of the polar angle.

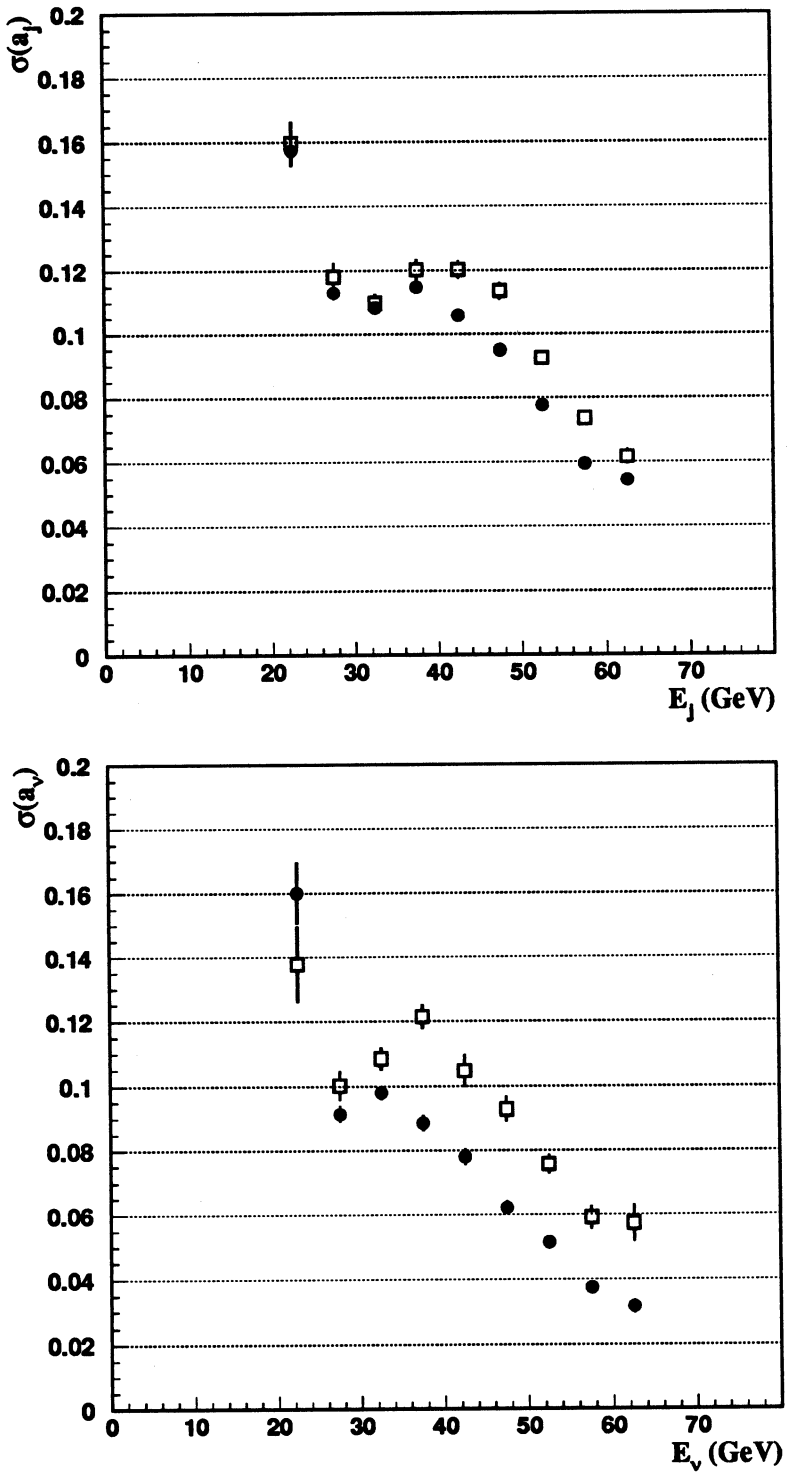

Figure 9: Resolution on the parameter **a** for jets and reconstructed neutrinos as a function of the energy, before(squares) and after 4-constrained fit(dots).

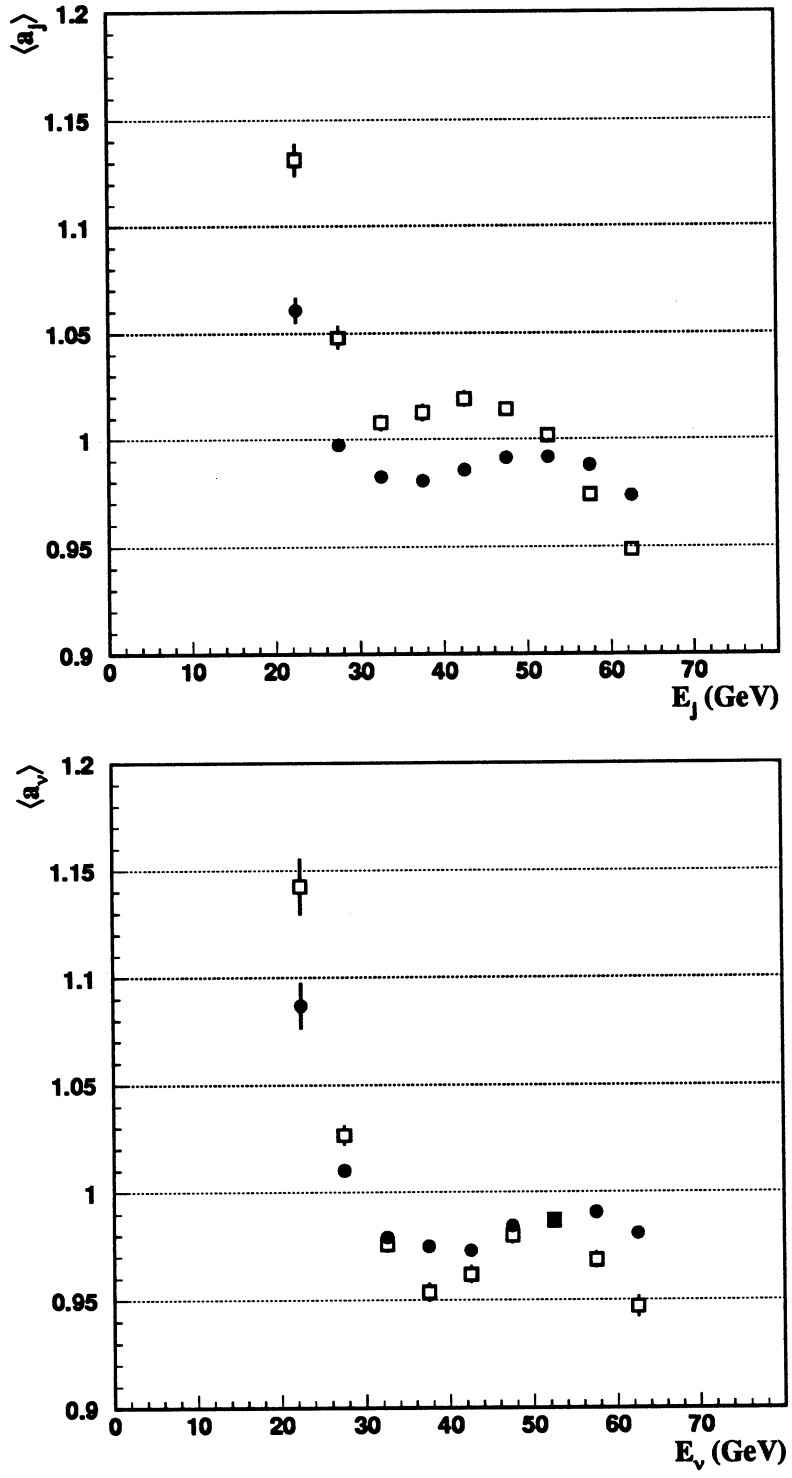

Figure 10: Mean value of **a** for jets and reconstructed neutrinos as a function of the energy, before(squares) and after the 4-constrained fit(dots).

which allows the fit to converge quickly in few iterations (2 or 3), but rather as:

$$f_5 = g(E_W - E_{beam}) = 0 \tag{3}$$

where $g(x)$ is a function close to 0 for small values of x. For instance $g(x) \propto x^p, p > 1$,[2] ($p = 5$ is used in this study). This makes the method converge much more slowly. The number of iterations is chosen so that the width of the fitted W energy distribution is equal to the expected (generated) one, $\Gamma_E = 2.18$ GeV$\simeq \Gamma_W$ (table 11).

Number of iterations	7	**8**	9
Γ_E (GeV)	3.09	**2.35**	1.93

Table 11: Width of the fitted W enregy as a function of the number of iterations.

Figure 13 shows that the resolution on the neutrino momentum is improved by almost a factor 2, while this factor is 1.5 for the jets. As shown in figures 11 , 12 and 13, the dependence upon the polar angle is reduced and the fitted energy is closer to the real one (a is closer to 1).

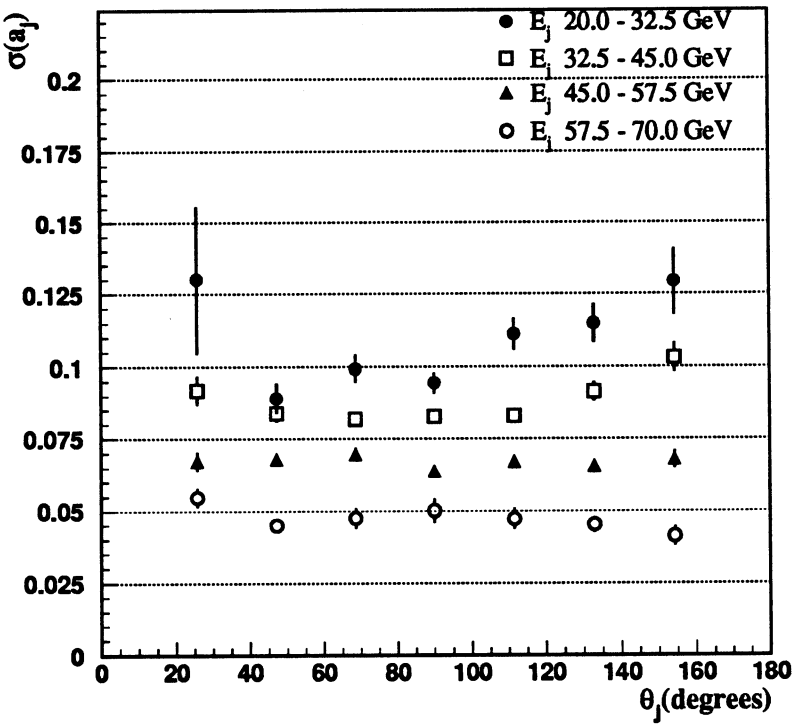

Figure 11: Resolution on the parameter **a** for jets in the $WW \to e, \mu\bar{\nu}q_1\bar{q}_2$ channel as a function of the polar angle after 5-constrained fit.

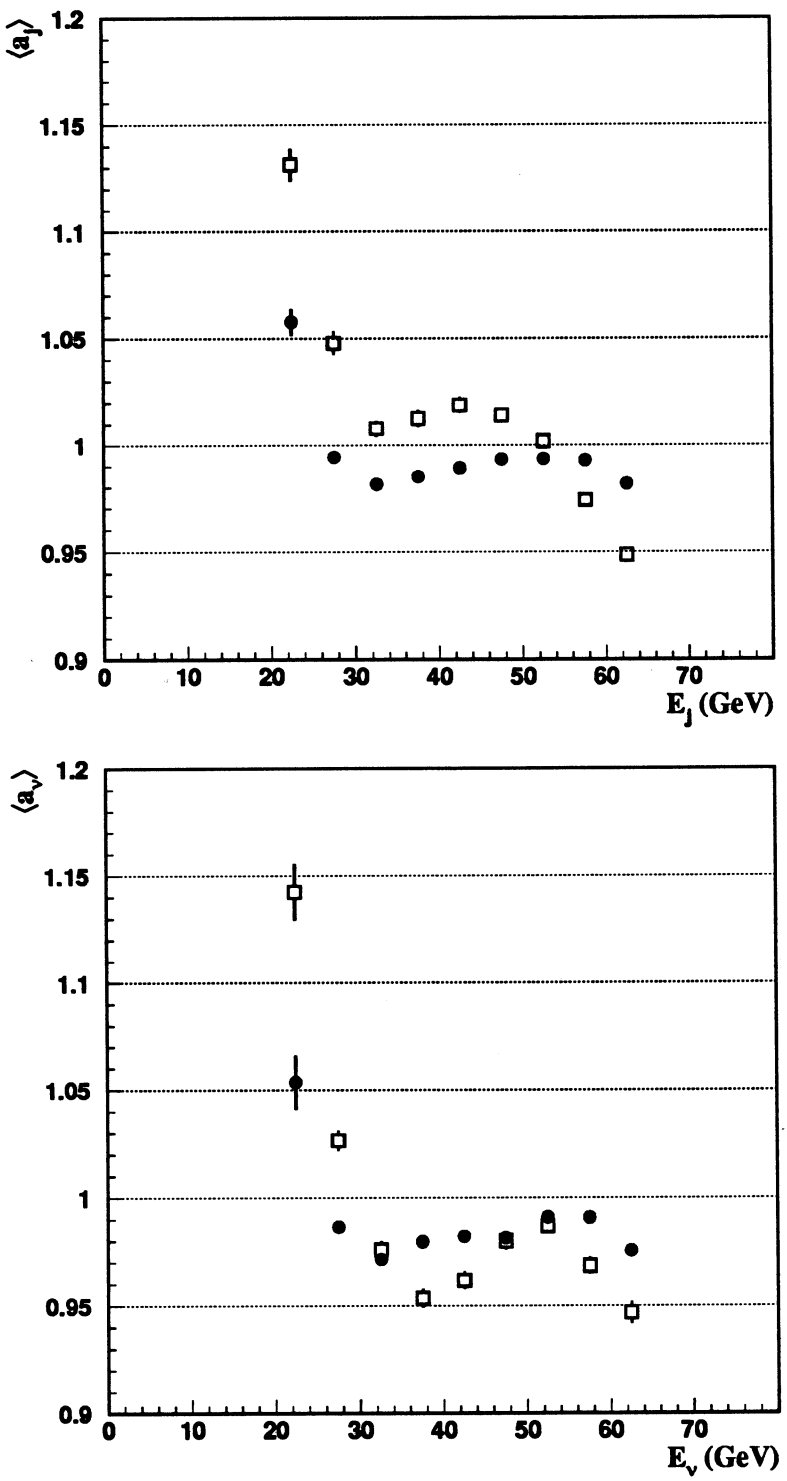

Figure 12: Mean value of **a** for jets and reconstructed neutrinos as a function of the energy, before(squares) and after 5-constrained fit(dots).

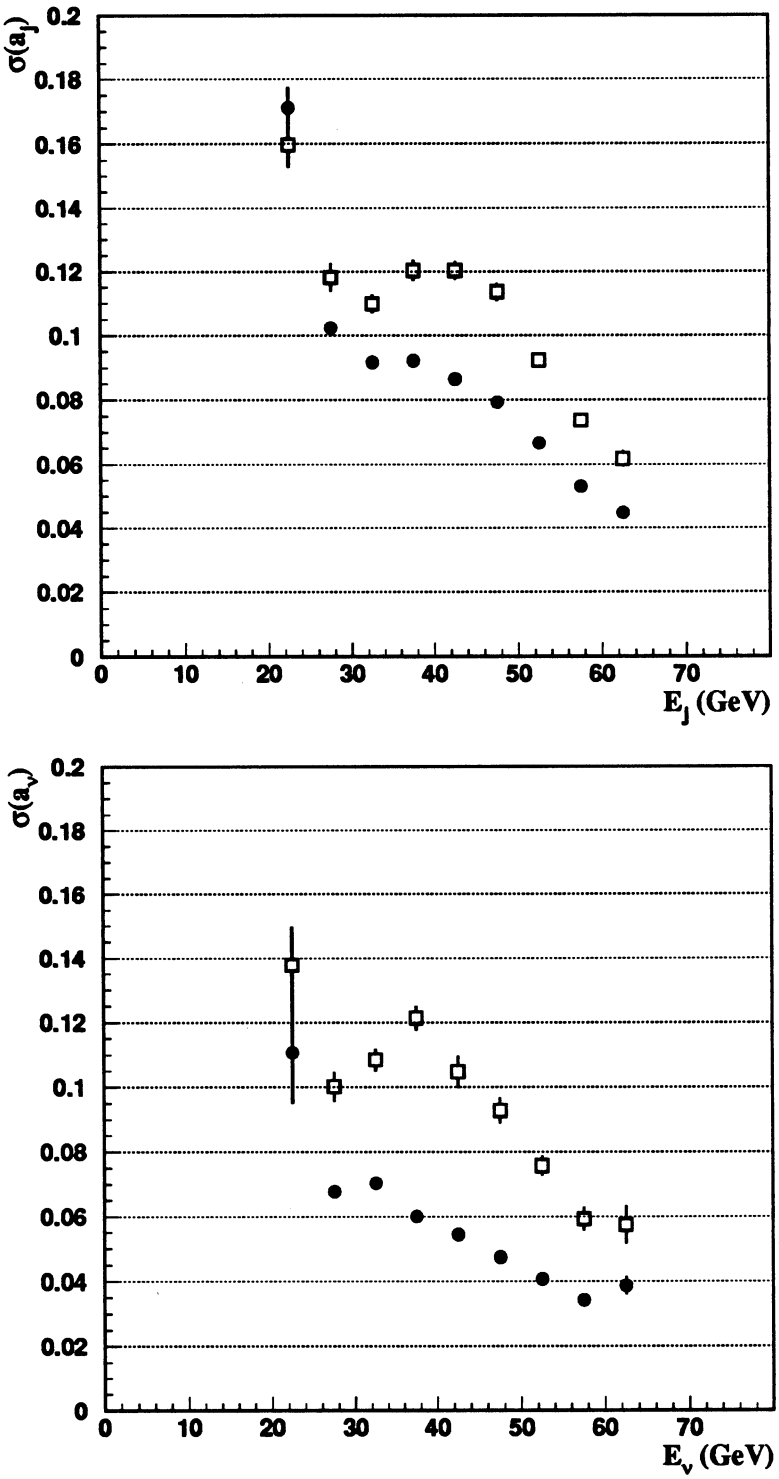

Figure 13: Resolution on the parameter **a** for jets and reconstructed neutrinos as function of the energy, before(squares) and after 5-constrained fit(dots).

5 W mass reconstruction

5.1 Methods

Three methods are used to measure the W mass:

- The event is not fitted, the scaled mass is defined as [1]:

$$m_W^s = m_W \times \frac{E_{beam}}{E_W} = E_{beam} \times \sqrt{1 - \frac{P_W^2}{M_W^2}} \tag{4}$$

  Where m_W is the mass obtained from the raw jets, or from the lepton-neutrino system when the lepton is an electon or muon.

- The event is fitted using the 4-constrained fit method, then the mass is scaled to obtain the W mass.

- The 5-constrained fit is applied without scaling the W mass.

Both hadronic and leptonic W's are used in the $WW \rightarrow e, \mu \bar{\nu} q_1 \bar{q}_2$ channel while only the hadronic W mass is fitted in the $WW \rightarrow \tau \bar{\nu} q_1 \bar{q}_2$ channel because of the degraded resolution on the lepton energy. A Breit-Wigner like function is used to fit the obtained mass distribution.

$$\frac{NM^2}{(M^2 - M_0^2)^2 + M^4\Gamma^2/M_0^2} \tag{5}$$

Because of the kinematical constraints, the mass distribution is not symmetric, and, as shown in figure 14, the result depends on the range of the fit, especially the upper bound, m^{up}. The statistical error on the W mass, ε, given by the fit decreases with m^{up}, as the fitted statistics increase. The fitted mass, m_{fit}, depends, also, on m^{up}, which leads to a high systematic error (25 MeV/c^2)[1].

Figure 15 shows that the χ^2_{fit} of the fit increases, until it reaches a region where it takes a constant value before increasing again. A method is developped to reduce this effect. The goal is to minimize the statistical error while keeping m_{fit} in the stable region and a low value for χ^2_{fit}. We minimize the following expression with respect to m^{up} :

$$\chi^2(m^{\mathrm{up}}) = \chi^2_{\mathrm{fit}}(m^{\mathrm{up}}) + \frac{(m_{\mathrm{fit}}(m^{\mathrm{up}}) - m_W^{\mathrm{max}})^2}{\Delta^2_{\mathrm{fit}}} + \frac{\varepsilon^2(m^{\mathrm{up}})}{\delta\varepsilon^2} \tag{6}$$

Where Δ_{fit} is the desired systematic error due to the fit (chosen here as 5 MeV/c^2), and m_W^{max} is the highest fitted mass taken as an arbitary reference to evaluate the variation of m_{fit}. $\delta\varepsilon$ is chosen equal to 5 MeV/c^2, in order to minimize the total error on the W mass (figure 15).

This method has the advantage to adapt, using Δ_{fit} and $\delta\varepsilon$, the systematic and the statistical errors for a given integrated luminosity in order to optimize the total error.

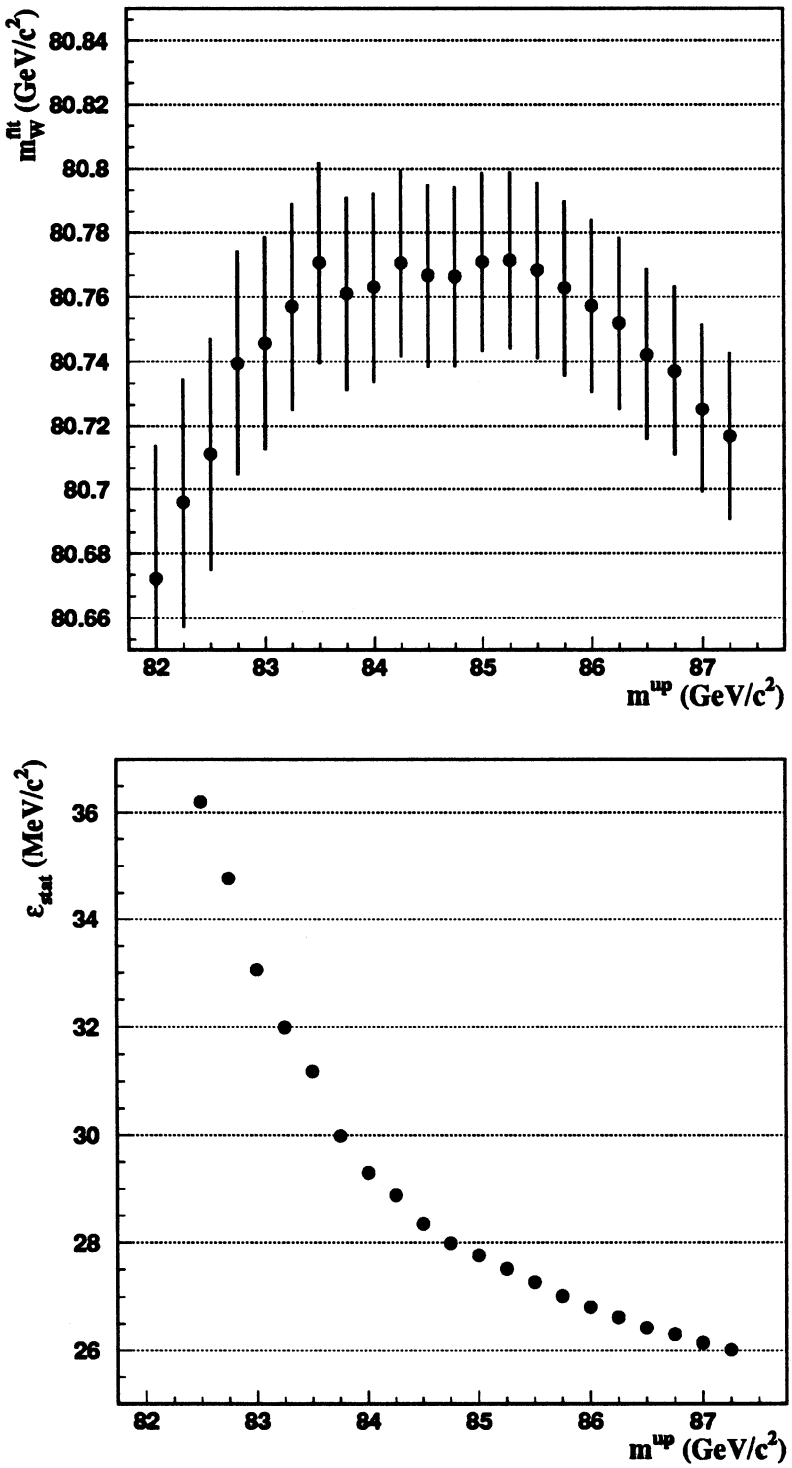

Figure 14: Fitted mass, m_W (a), and the statistical error on the W mass (b) as functions of the upper bound m^{up} at 176 GeV, a generated mass $M_W = 80.25$ GeV/c^2 and for 3200 pb^{-1}.

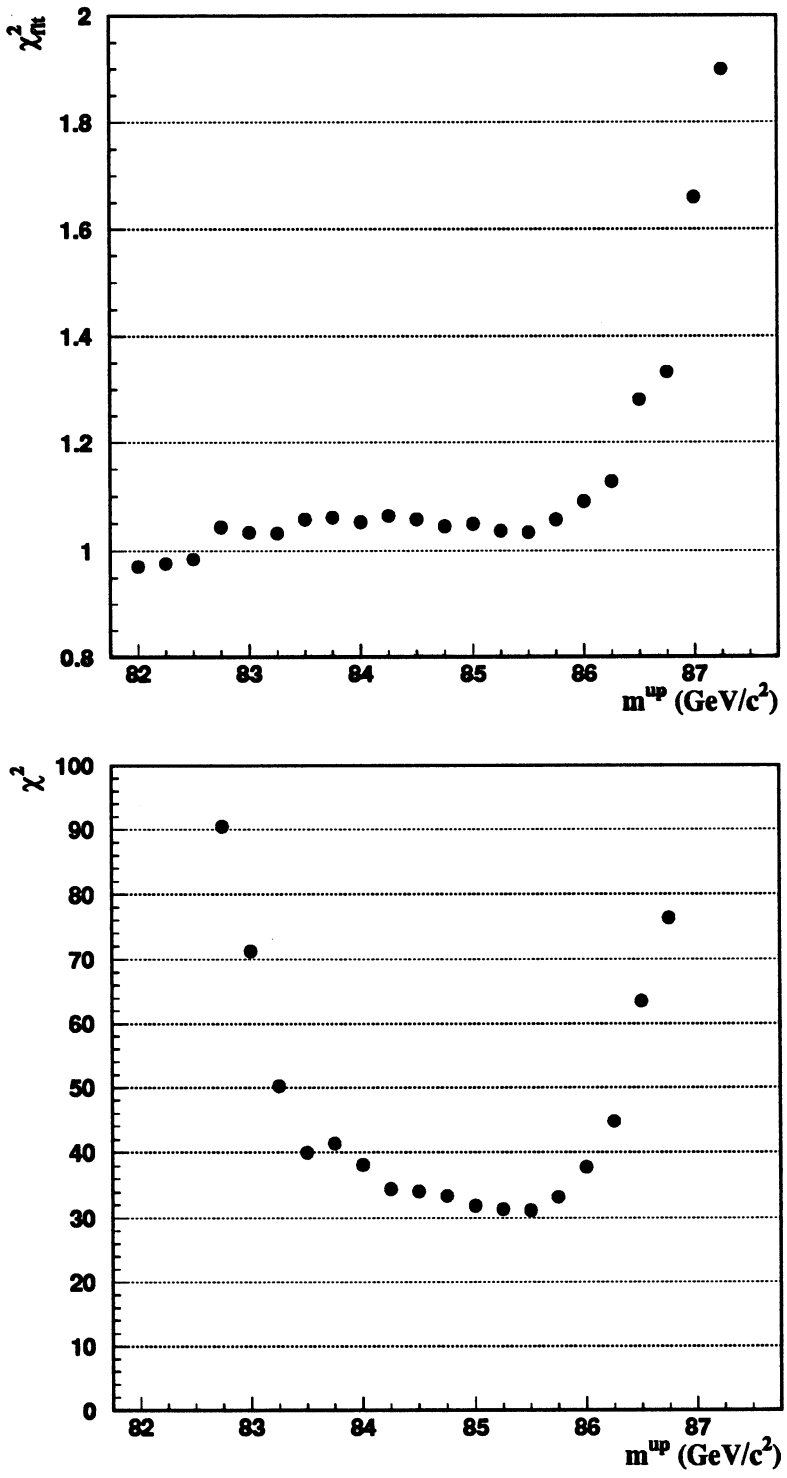

Figure 15: χ^2_{fit} of the fit (a) and the total χ^2 (b) as functions of the upper bound m^{up} at 176 GeV, a generated mass $M_W = 80.25$ GeV/c^2 and for 3200 pb^{-1}.

5.2 Results

The method with $\chi^2(m^{up})$ is used only for the $WW \to e,\mu\bar{\nu}q_1\bar{q}_2$ channel, because of the important low mass tail in the $WW \to \tau\bar{\nu}q_1\bar{q}_2$ channel (figure 16). This does not change the total systematic error as its effect is largely attenuated by the low statistics in this channel.

Tables 12 and 13 show the fitted masses after scaling in different channels with and without the 4-constrained fit. In the $WW \to e,\mu\bar{\nu}q_1\bar{q}_2$ channel, the average mass is calculated taking into account the correlation between the two scaled masses (table 14). Then the fitted masses from the two channels are combined.

The total statistical error is improved after the 4-constrained fit because of the better reconstruction of the leptonic system. However, despite the better energy reconstruction with the 5-constrained fit, the measured mass is not improved (table 15), especially in the $WW \to \tau\bar{\nu}q_1\bar{q}_2$ channel where the fifth constraint can not be fulfilled without distortion of the jet momenta.

		m_W (GeV/c^2)	Γ_W (GeV/c^2)
$WW \to e,\mu\bar{\nu}q_1\bar{q}_2$	m_{qq}	80.626 ± 0.027	4.036 ± 0.055
	$m_{\ell\nu}$	80.948 ± 0.035	5.193 ± 0.074
	Average	80.706 ± 0.026	
$WW \to \tau\bar{\nu}q_1\bar{q}_2$	m_{qq}	80.566 ± 0.065	4.697 ± 0.150
Average mass		80.687 ± 0.024	

Table 12: Fitted mass without event fit and after scaling, for 3200 pb^{-1} at 176 GeV and a generated mass $M_W = 80.25$ GeV/c^2

		m_W (GeV/c^2)	Γ_W (GeV/c^2)
$WW \to e,\mu\bar{\nu}q_1\bar{q}_2$	m_{qq}	80.841 ± 0.026	3.792 ± 0.051
	$m_{\ell\nu}$	80.841 ± 0.030	4.654 ± 0.068
	Average	80.841 ± 0.024	
$WW \to \tau\bar{\nu}q_1\bar{q}_2$	m_{qq}	80.812 ± 0.067	4.665 ± 0.155
Average mass		80.838 ± 0.023	

Table 13: Fitted mass after 4-constrained fit and scaling, for 3200 pb^{-1} at 176 GeV and a generated mass $M_W = 80.25$ GeV/c^2

method	1st	2nd	3rd
correlation ρ	0.51	0.58	0.83

Table 14: Correlation factor between the two masses in the $WW \to e,\mu\bar{\nu}q_1\bar{q}_2$, for 3200 pb^{-1} at 176 GeV and a generated mass $M_W = 80.25$ GeV/c^2

Table 16 shows the measured masses, for two other generated M_W, using the 3 methods. The relative mass shifts shown in table 17 are in agreement with the generated

		m_W (GeV/c^2)	Γ_W (GeV/c^2)
$WW \to e,\mu\bar{\nu}q_1\bar{q}_2$	m_{qq}	80.737 ± 0.030	4.255 ± 0.063
	$m_{\ell\nu}$	80.640 ± 0.031	4.601 ± 0.065
	$(m_{qq}+m_{\ell\nu})/2$	80.689 ± 0.025	3.823 ± 0.055
$WW \to \tau\bar{\nu}q_1\bar{q}_2$	m_{qq}	80.494 ± 0.098	5.776 ± 0.290
Average mass		80.677 ± 0.024	

Table 15: Fitted mass after 5-constrained fit, for 3200 pb^{-1} at 176 GeV and a generated mass M_W = 80.25 GeV/c^2.(In the $WW \to e,\mu\bar{\nu}q_1\bar{q}_2$ channel the average is computed event by event).

ones. However, table 18 shows that the absolute mass shift depends on the center of mass energy. The statistical error is not optimized for 165 and 190 GeV, as we use a covariance matrix obtained at 176 GeV.

Generated mass	80.00(GeV/c^2)	80.25(GeV/c^2)	80.50 (GeV/c^2)
1st method	80.370 ± 0.034	80.687 ± 0.024	80.913 ± 0.033
2nd method	80.538 ± 0.034	80.838 ± 0.023	81.068 ± 0.032
3rd method	80.371 ± 0.037	80.677 ± 0.024	80.956 ± 0.034

Table 16: Fitted mass as a function of the generated one at 176 GeV.

Generated mass shift	-250 (MeV/c^2)	+250 (MeV/c^2)
1st method	-317 ± 42	+226 ± 41
2nd method	-300 ± 41	+230 ± 39
3rd method	-306 ± 44	+279 ± 42

Table 17: Mass shift for the three methods(obtained from table 16) at 176 GeV.

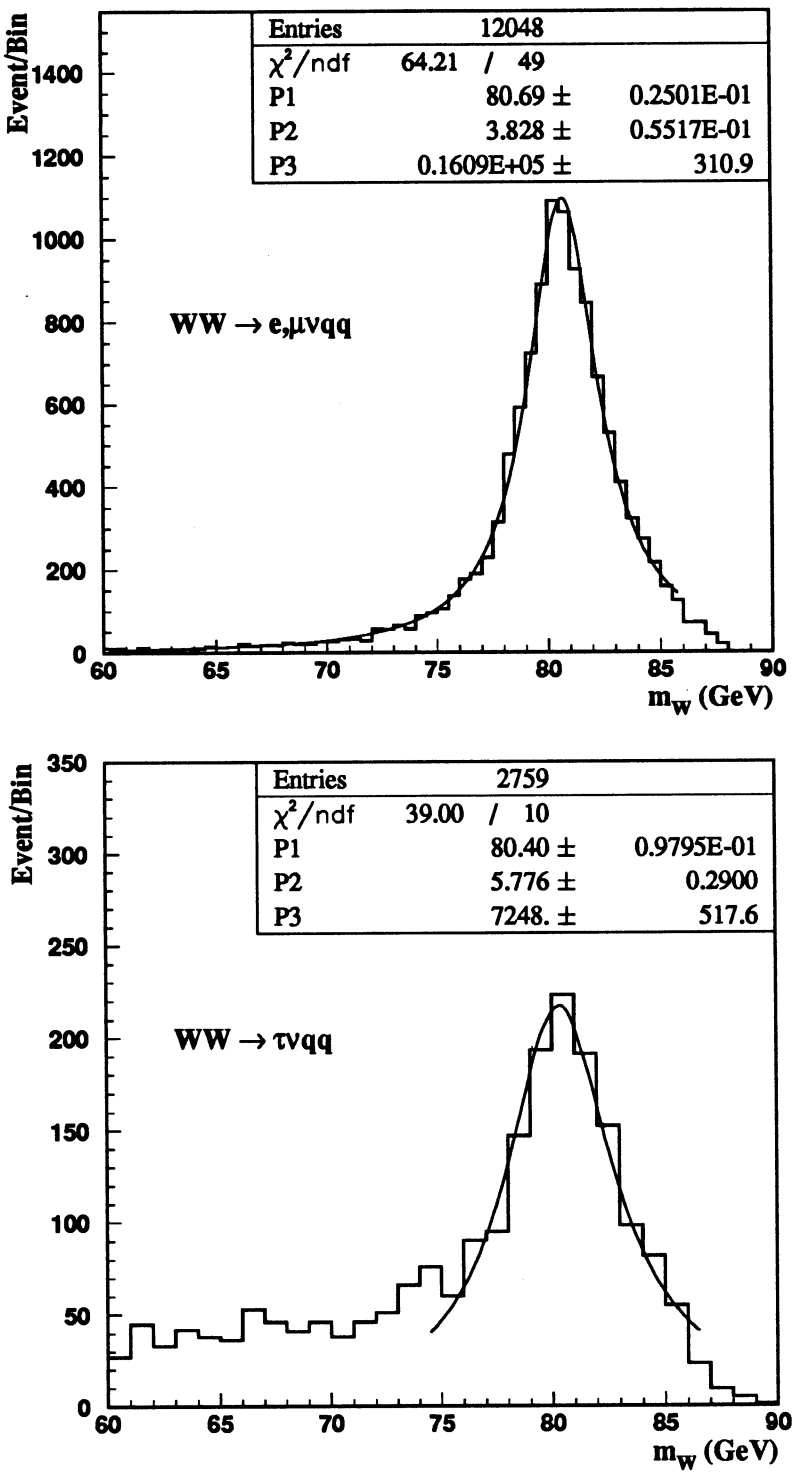

Figure 16: Mass distribution after 5-constrained method at 176 GeV, from a generated mass $M_W = 80.25$ GeV/c^2 and for 3200 pb^{-1}.

LEP energy	165 GeV	176 GeV	190 GeV
1^{st} method	80.465 ± 0.069	80.687 ± 0.024	81.100 ± 0.042
2^{nd} method	80.339 ± 0.042	80.838 ± 0.023	81.597 ± 0.044
3^{rd} method	80.000 ± 0.048	80.677 ± 0.024	81.292 ± 0.042

Table 18: Fitted mass as a function of center of mass energy for a generated W mass m_W=80.25 GeV/c^2.

6 Conclusion

A very clean selection, independent of the center of mass energy, can be obtained in the $WW \to \ell\bar{\nu}q_1\bar{q}_2$ channel (85% of the $WW \to e, \mu\bar{\nu}q_1\bar{q}_2$ with a purity of 96% and 33% of the $WW \to \tau\bar{\nu}q_1\bar{q}_2$ with a purity of 92%). The resolution on the jet and neutrino momenta is improved using the constrained fit method, which allows a better mass reconstruction. The 4-constrained fit (plus the mass scaling) gives the best statistical error. Table 19 shows the statistical errors for 500 pb^{-1} at different center of mass energies. A new fit procedure of the mass distribution reduces further the systematic error due to fit from 25 MeV to 5 MeV.

LEP energy (GeV)	165	176	190
Statistical error (MeV/c^2)	100 ± 2.5	59 ± 1.	71± 2.

Table 19: Statistical error on the W mass as a function of center of mass energy for 500 pb^{-1}

References

[1] **P. Perez and J. Schwindling**
W mass reconstruction at LEP 200
ALEPH 93-113(PHYSIC 93-94)

[2] **A. Trabelsi, P. Perez and J. Schwindling**
W mass reconstruction at LEP 200 using WW→QQQQ events
ALEPH 94-73 (PHYSIC 94-62)

[3] **LL. M. Mir**
W mass fit from qqqq
ALEPH week, INNSBRUCK, september 1993

[4] **DELPHI Collaboration**
Reconstruction of invariant masses of multi-jet events
DELPHI 91-17 (PHYS 88)